An investigation of dynamic behaviour of cracked porous graded moving plate under thermal environment

Rusul J. Manshad, Talib EH. Elaikh

Mechanical Engineering Department, College of Engineering, University of Thi-Qar, Iraq.

Abstract
The vibration characteristic of a cracked porous graded moving plate based on a neutral surface plane under uniform temperature rise is investigated in this paper. The material property gradient is based on the distribution of the power law in the direction of the plate thickness. The vibration equation is obtained depending on the classical plate theory (CPT), and resolved by the extension of the Differential quadrature approach (DQM). Furthermore, the mode shapes of the model are determined for simply supported moving graded plates with cracks. The present natural frequencies results are compared with those available in the published literature and a good agreement is found. The effect of key parameters such as plate velocity, crack length ratio, gradient index, and porosity on the dynamic characteristics of axial moving systems in addition to their physical interpretations is described.

Keywords: Classical plate theory (CPT); DQM; crack FGM porous plate; Axially Moving.

1. Introduction
These instructions give you the guidelines for preparing papers for IJEE. Use this document as a template. To ensure publication quality and uniformity, the following requirements have been prepared to assist authors in preparing papers for the journal. If these requirements are not followed, papers will be returned for revision and re-submittal.
Functionally graded (FG) thin plates with longitudinal motion have many applications in various engineering fields. These plates may be subjected to mechanical or thermal loads, and therefore defects may occur as a result of these loads. These defects can be in the form of a crack on the surface, an internal crack, or any type of defect. The presence of cracks in plate structures causes changes in their physical characteristics such as stiffness, mass, and consequently changes in vibrational characteristics, such as natural frequencies and the shape of modes. Therefore, analysis and knowledge of the behavior of these structures is of great importance. In this regard, very extensive studies on the vibration of FGM plates have been conducted by many researchers. For example, [1] analyzed the free vibration, and buckling of FGM thin plate based on the classical theory of the plate and the neutral surface position. A theoretical analysis was presented to find the vibration frequency and critical bucking loading. [2], studied the free vibration of a FGM rectangular plate based on the theory of first-order shear deformation. In this study, they examined four types of functionally graded materials. [3], studied the free vibrations of an exponential

graded rectangular plate in a thermal environment based on the classical theory of plates. Rayleigh-Ritz method was utilized to find vibration frequency.

On the other hand, the appearance of small pores inside the functionally graded material (FGM) was observed during the preparation process, which had a significant impact on the physical characteristics and static and dynamic characteristics of FGM. Therefore, in recent years, it has attracted the attention of researchers in studying the effect of these pores on the mechanical behavior of FGM structures containing pores. For example, [4] used the finite element method to study the free vibration and static characteristics of the porous FG magneto-electric elastic plate. The modified mixing ratio formula is mainly used to analyze the influence of the porosity distribution on the structural performance of the plate and the effect on the vibration and static characteristics of the plate. The free vibrations of the porous rectangular plates were studied by [5]. Based on the TSDT and Hamilton's principle, the vibration equation were derived. An analytic solution with the application of Levi's solution was used to solve ordinary differential equations. The vibration characteristic of rectangular porosity FG plates was investigated by [6]. The equation of motion was derived based on Hamilton's principle and FSDT. According to the modified power law, the physical properties of the plate were graded in thickness direction were assumed.

For axial moving structures, many researchers have done some research on plates made of traditional isotropic materials, but there are few studies on functionally graded material (FGM) plates with axial motion. [7], used the differential quadrature method to analyze the inherent characteristics of the viscoelastic axially moving plate. The relationship curves among the critical velocity, the dimensionless vibration frequency and the aspect ratio, the dimensionless motion speed, and the dimensionless stiffness of the four-sided simply supported axially moving thin plate was plotted. [8], based on the D'Alembert principle, vibration equation was derived for nonlinear vibration of axial movement FGM plate. The harmonic balance method are used to analyze the vibration frequency and nonlinear dynamic response of the plate under four-sided simply supported boundary conditions. [9], based on classical plate theory, the dynamic behavior of an axially moving plate under the influence of surrounding axial airflow has been studied. [10], based on D'Alembert principle, the equation of motion was derived taking into account the thermal effects and motion axially. Galerkin's methods and harmonic equilibrium were used to solve the ODE. [11], studied the vibration characteristics of axially moving plates partially immersed in fluid on the basis of classical thin plate theory. The results showed that the vibration characteristics are affected by the speed of movement as well as the fluid and plate density ratios. [12], used assumed mode method to study the vibration characteristics of the axially moving FGM plate with aero-thermal environment. Based on the classic plate theory and the Hamilton principle, the vibration equation were derived. [13], investigated the dynamic characteristic and stability of a thermoplastic coupling moving rectangular plate. The thermoplastic coupling differential equation for a moving plate was obtained by integrating the thermoplastic conduction equation. A new analytical model for free vibration analysis of a simply supported rectangular functionally graded sandwich plate was presented by [14]. Theoretical formulations are based on the classical plate theory to find the free vibration characteristics of the imperfect and perfect FGM sandwich plate. To validate the analytical solution, finite element analysis (FEA), as well as ANSYS-2020-R2 software, were used. The results reveal that the frequency parameter of the sandwich plate increases with the increase of the porosity parameter and number of the constraints in the boundary conditions. [15] presented a new approximated analytical solution of the free vibration analysis of functionally graded rectangular sandwich plates with porosities. The kinematic relations were developed based on the classical plate theory (CPT), and the governing differential equation is derived by employing the Rayleigh-Ritz approximate method. The influences of changing the gradient index, porosity distribution, boundary conditions, and geometrical properties on the free vibration characteristics were analyzed.

Additionally, the presence of cracks in plate structures causes changes in vibrational characteristics, such as natural frequencies and the shape of modes. Therefore, modeling defective structures in order to fully understand the nature of the defect, has caused increasing attention of researchers. Firstly, [16], studied the stress factor of a rectangular fracture plate under the simultaneous effect of tensile and flexural loads. The crack was considered as a local decrease in the stiffness of the plates, and the crack was modeled using tension and torsion springs. [17], investigated the vibrational behavior of cracked plates with intermediate cracks, of the desired direction and length. For this purpose, with the help of Kirchhoff's theory, the governing equations of the cracked plate were extracted, and then, a method of multi-scale was used to solve the obtained equation. [18] modeled the crack as a torsion spring, and the vibrational behavior of the rectangular plate with the overall crack was investigated. Open crack was assumed and the plate was

divided into two parts along the crack. Then, by applying the appropriate boundary conditions, the differential equations of the vibrations of each part of the plate were extracted. [19], presented an analytical solution to find the vibration frequency of crack isotropic composite plates. The natural frequency of the powder- and short-fiber-reinforced composite was investigated. [20], investigated the dynamic behavior of moving Rayleigh graded beam with an edge crack. Hamilton's precept was used to obtain the motion equation of the system. A rotational massless spring was used to model the crack. [21], investigated the thermal effects on the vibrations of the rectangular isotropic plate. Using classical plate theory and Burger's nonlinear formula, they investigated the effects of crack-temperature bonding on dynamic properties. [22], predicted the frequency of an FGM plate with evenly distributed porosity and a lateral superficial crack simply supported FGM plate. The FGM plate motion equations were derived using TSDT.

In light of the above reviews, and to the best of the author's knowledge it was noted that the dynamic behavior of a cracked porous gradient plate with axial motion has not yet been studied. Therefore, the importance and novelty of this study lies in the study of free vibrations of porous cracked plates which is a new topic in this field. Since both crack and porosity influence the vibration characteristics of a moving FGM plate, the current study attempts to demonstrate these effects. In this work, the classical plate theory with the concept of a neutral normal surface was used to derive the equation of motion. The obtained vibration equation is solved using the differential quadrature method. The effects of several variables on vibration properties were observed, including porosity, crack length, axial velocity, and material property gradient index.

2. Mathematical Formulation

Figure (1) displays a schematic diagram of the moving graded thin plate. Set its length as l_1, width as l_2, and thickness as h. It moves longitudinally with uniform speed V. $2a$ is the crack length, and C_d is the crack depth. In this study, the volume fraction, in the plate thickness, is constantly changing. Depending on the power-law gradient, the volume ceramic fraction is [23],

$$V_c = (z/h + 0.5)^k \tag{1}$$

Where, ($k \geq 0$) is the material composition index. The effective material properties of porous plates with even porosities (i.e. equivalent elastic modulus $E(z)$, thermal expansion coefficient $\alpha(z)$, mass density $\rho(z)$, can be expressed as, [24],

$$E(z) = E_m + (E_c - E_m)(0.5 + z/h)^k - \frac{\beta}{2}(E_c + E_m) \tag{2}$$

$$\rho(z) = \rho_m + (\rho_c - \rho_m)(0.5 + z/h)^k - \frac{\beta}{2}(\rho_c + \rho_m) \tag{3}$$

$$\alpha(z) = \alpha_m + (\alpha_c - \alpha_m)(0.5 + z/h)^k - \frac{\beta}{2}(\alpha_c - \alpha_m) \tag{4}$$

Figure 2 exhibits the contrast of perfect FGM and FGM with porosity $\beta = 0.2$ versus the direction of plate thickness for different index gradients. From this figure, it can be seen that porosity FGM has a lower Young's modulus as compared to a perfect FGM.

Based on the classic thin plate small deflection deformation theory, ignoring the influence of transverse shear strain, and taking the neutral surface of the plate into account, the displacement field at any point of the FGM plate is,

$$u = -(z - z_o)\frac{\partial w}{\partial x}, \quad v = -(z - z_o)\frac{\partial w}{\partial y}, \quad w = w(x, y) \tag{5}$$

Where, u, v, and w respectively denote the neutral displacements of the plate along x, y, and z axes, and z_o is presented to explain the neutral position, given by [1],
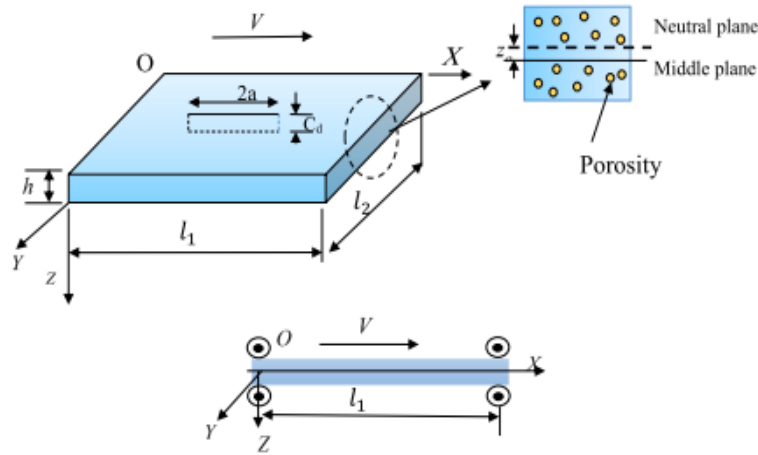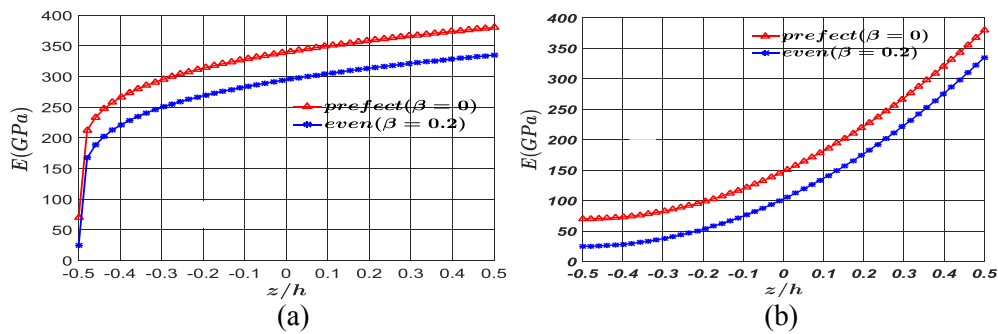
Figure 1. FG porous moving plate model.

(a)   (b)

Figure 2. Perfect and porous FGM Young's modulus variations with $\beta = 0.2$ a)$k = 0.2$; b)$k = 2$.

$$z_o = \int_{-h/2}^{h/2} zE(z)dz / \int_{-h/2}^{h/2} E(z)dz \qquad (6)$$

So, neglecting a temperature environment, the strain related to the displacement above can also be rewritten as,

$$\varepsilon_x = \frac{\partial u(x,y,z,t)}{\partial x} \ , \ \varepsilon_y = \frac{\partial v(x,y,z,t)}{\partial y} \ , \ \gamma_{xy} = (\frac{\partial u(x,y,z,t)}{\partial y} + \frac{\partial v(x,y,z,t)}{\partial x}) \qquad (7)$$

In which ε_x and ε_y are the normal strains, and γ_{xy} is the in-plane shear strain. By assuming that the material components of the FG plate comply with Hooke's generalized law, the stress-strain constitutive relationship of the axially moving FGM thin plate is,

$$\sigma_{xx} = \frac{E(z)}{1-v^2}\left(\varepsilon_x + v\varepsilon_y\right), \ \sigma_{yyx} = \frac{E(z)}{1-v^2}\left(\varepsilon_y + v\varepsilon_x\right), \ \tau_{xy} = \frac{E(z)}{1-v^2}\left(\frac{1-v}{2}\right)\gamma_{xy} \qquad (8)$$

2.1. Formulation of in-plane forces and moment
In absence of temperature, Figure 3 shows the internal forces and bending moments that affect the FG thin plate element. After analyzing the forces in the z-direction and bending moment in x, y-direction, taking equilibrium in the x and y-axis, as well as simplification, neglecting the higher-order quantity, the moment equations in the x, y-direction, can be written as,

$$\frac{\partial^2 M_x}{\partial x^2} + 2\frac{\partial^2 M_{xy}}{\partial x \partial y} + \frac{\partial^2 M_y}{\partial y^2} = I_o \frac{\partial^2 w}{\partial t^2} \tag{9}$$

In which M_x, M_y and $M_{xy} = M_{yx}$ are bending moments and moment of twist per unit length

respectively, $M_x = \int_{-h/2}^{h/2} \sigma_x (z - z_o)dz$, $\qquad M_y = \int_{-h/2}^{h/2} \sigma_y (z - z_o)dz$,

$M_{xy} = \int_{-h/2}^{h/2} \tau_{xy}(z - z_o)dz$, $I_o = \int\limits_{-h/2}^{h/2} \rho(z)\ dz = \rho_m h \alpha$

The total derivative of the right-side term due is written as [11],

$$\frac{\partial^2 w}{\partial t^2} = V^2 \frac{\partial^2 w}{\partial x^2} + 2V \frac{\partial^2 w}{\partial x \partial t} + \frac{\partial^2 w}{\partial t^2} \tag{10}$$
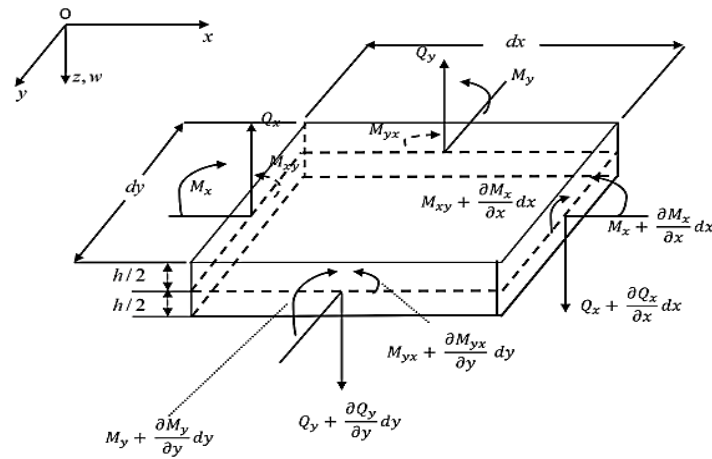

Figure 3. Physical model of the functionally graded plate with axial motion.

In the case of temperature, the membrane force due to temperature change shown in Figure 4 that affects the thin plate element FG is taken into account. Since the in-plane shear strength of the thin sheets is not affected by the temperature change, so the shear force is ignored [21]. Thermal stress coefficients under uniform temperature rise, for the FG thin plate, can be explicit as [21],

$$\sigma_{Tx} = \frac{E(z)\alpha(z)\Delta t}{1-v}, \ \sigma_{Ty} = \frac{E(z)\alpha(z)\Delta t}{1-v}, \ \tau_{Txy} = 0 \tag{11}$$

Using the thermal stress parameters above, the moments in terms of w is written as,

$$M_x = -EI_{eq}\left(\frac{\partial^2 w}{\partial x^2} + v\frac{\partial^2 w}{\partial y^2}\right) - M_T$$

$$M_{xy} = -EI_{eq}(1-v)\frac{\partial^2 w}{\partial x \partial y}$$

$$M_y = -EI_{eq}\left(\frac{\partial^2 w}{\partial y^2} + v\frac{\partial^2 w}{\partial x^2}\right) - M_T \tag{12}$$

Where, $M_T = \int\limits_{-h/2}^{h/2} \dfrac{E(z)z\alpha(z)}{(1-v)}\Delta T dz$ is   thermal   moment   And,

$$EI_{eq} = \int\limits_{-h/2}^{h/2} B(z-z_o)^2 dz = D_c\gamma, \quad D_c = \dfrac{E_c h^3}{12(1-v^2)}$$

For in plane temperature force, consider the plate element's equilibrium $dxdy$ as depicted in Figure 4. In this work, the equilibrium adopted by [21] is used for in-plane temperature compressive forces. By taking the equilibrium in the z-axis, ignoring the higher-order conditions, the in-plane transverse forces are written as,

$$\sum F_z(x,y) = -N_{Tx}\dfrac{\partial^2 w}{\partial x^2} - \left(N_{Ty}\dfrac{\partial^2 w}{\partial y^2} + \overline{N}_y\dfrac{\partial^2 w}{\partial y^2} \right) \tag{13}$$

Where $\overline{N}_y$ is the additional crack membrane force [25]. The in-plane forces due to the uniform temperature rise N_{Tx} and N_{Ty}, are given as,

$$N_{Tx} = N_{Ty} = \int\limits_{-h/2}^{h/2} \dfrac{E(z)\alpha(z)}{(1-v)}\Delta T dz = N_T\gamma_1 \tag{14}$$

By adding of the forces given by Eq. (13) and substituting the moments Equation (12) into Eq. (9), the vibration equation of cracked FG plate as,

$$EI_{eq}\left(\dfrac{\partial^4 w}{\partial x^4} + 2\dfrac{\partial^4 w}{\partial x^2\partial y^2} + \dfrac{\partial^4 w}{\partial y^4} \right) = -I_o\dfrac{\partial^2 w}{\partial t^2} - \dfrac{\partial^2 M_T}{\partial x^2} - \dfrac{\partial^2 M_T}{\partial y^2} + \dfrac{\partial^2 \overline{M}_y}{\partial y^2}$$
$$- N_{Tx}\dfrac{\partial^2 w}{\partial x^2} - N_{Ty}\dfrac{\partial^2 w}{\partial y^2} - \overline{N}_y\dfrac{\partial^2 w}{\partial y^2} \tag{15}$$
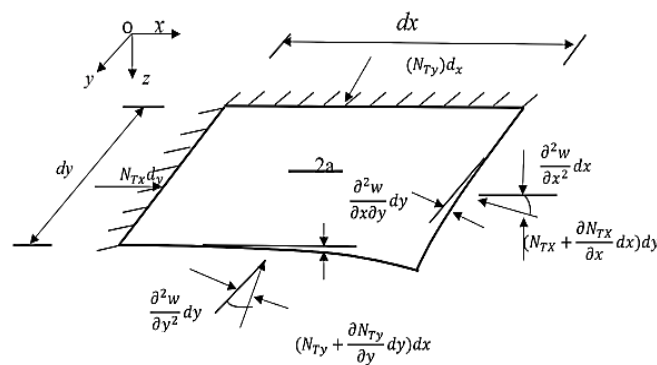

Figure 4. Plate element in-plane thermal forces with 2a-length crack.

Substituting Eq. (10) into Eq. (15), the vibration equation of cracked FG plate is written as,

$$EI_{eq}\left(\dfrac{\partial^4 w}{\partial x^4} + 2\dfrac{\partial^4 w}{\partial x^2\partial y^2} + \dfrac{\partial^4 w}{\partial y^4} \right) = -I_o\left(V^2\dfrac{\partial^2 w}{\partial x^2} + 2V\dfrac{\partial^2 w}{\partial x\partial t} + \dfrac{\partial^2 w}{\partial t^2} \right) - \dfrac{\partial^2 M_T}{\partial x^2}$$
$$- \dfrac{\partial^2 M_T}{\partial y^2} + \dfrac{\partial^2 \overline{M}_y}{\partial y^2} - N_{Tx}\dfrac{\partial^2 w}{\partial x^2} - N_{Ty}\dfrac{\partial^2 w}{\partial y^2} - \overline{N}_y\dfrac{\partial^2 w}{\partial y^2} \tag{16}$$

2.2. Crack terms equation

Several studies about the plates exposed to cracks, as well as the modeling of these cracks, have been presented by a number of researchers and one of the most important modeling methods are those presented by [26, 27] which are represented by crack representation based on the spring line model (LSM) and, consequently, the internal forces and moments that occurred as a result of which the cracks were added. Figure 5 shows, on both sides of the crack site, the stress σ_{rs} and the bending stress m_{rs}, respectively. The equations for these stresses are written as [17],

$$\sigma_{rs} = \frac{N_{rs}}{h} = \frac{1}{h}\int_{-h/2}^{h/2}\tau_{rs}(x,y,z)dz$$
$$m_{rs} = 6\frac{M_{rs}}{h} = \frac{6}{h^2}\int_{-h/2}^{h/2}z\tau_{rs}(x,y,z)dz \qquad (17)$$

The tensile and bending stresses relationship in the plate afar sides (σ_{rs}, m_{rs}) and the location of the crack ($\overline{\sigma}_{rs}, \overline{m}_{rs}$) is obtained as follows [26],

$$\overline{\sigma}_{rs} = \frac{2a}{(6a_{tb}+a_{tt})(1-v^2)h+2a}\sigma_{rs}$$
$$\overline{m}_{rs} = \frac{2a}{3(\frac{a_{bt}}{6}+a_{bb})(3+v)(1-v)h+2a}m_{rs}$$

The tensile strength and moment due to a crack can be expressed along the y-axis,

$$\overline{N}_y = \frac{2a}{(6a_{tb}+a_{tt})(1-v^2)h+2a}N_{rs}$$
$$\overline{M}_y = \frac{2a}{3(\frac{a_{bt}}{6}+a_{bb})(3+v)(1-v)h+2a}M_{rs} \qquad (18)$$
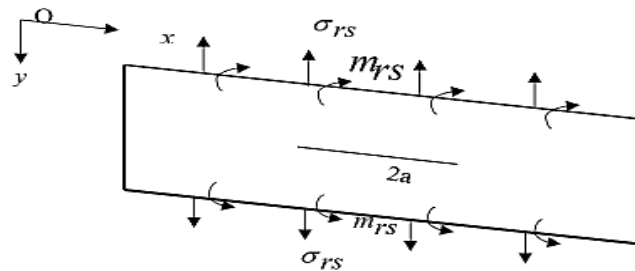

Figure 5. Tensile and bending stresses on the plate for a 2a part-through crack.

As a result of reducing of the total stiffness caused by crack, equations (18) are added with a negative sign. These two terms are given as follows [24, 26],

$$\overline{N}_y = -\overline{N}_{rs} = -\frac{2a}{(6a_{tb}+a_{tt})(1-v^2)h+2a}N_y^T \qquad (19)$$

$$\overline{M}_y = -\overline{M}_{rs} = -\frac{2a}{3(\frac{a_{bt}}{6}+a_{bb})(3+v)(1-v)h+2a}(M_y) \qquad (20)$$

The compliance coefficients are proportional to the crack depth ratio $\delta = C_d / h$, and they disappear when $C_d = 0$. The required compliance coefficient expressions are as follows [26],

$$a_{tt} = 1.154\delta^2 (1.98 - 0.54\delta + 18.65\delta^2 - 33.70\delta^3 + 99.26\delta^4 \\ - 211.90\delta^5 + 436.84\delta^6 - 460.48\delta^7 + 289.98\delta^8) \tag{21}$$

$$a_{bb} = 1.154\delta^2 (1.98 - 3.28\delta + 14.43\delta^2 - 31.26\delta^3 + 63.56\delta^4 \\ - 103.63\delta^5 + 147.52\delta^6 - 127.69\delta^7 + 61.50\delta^8) \tag{22}$$

$$a_{bt} = a_{tb} = 1.154\delta^2 (1.98 - 1.91\delta + 16.01\delta^2 - 34.84\delta^3 + 83.93\delta^4 \\ - 153.65\delta^5 + 256.72\delta^6 - 244.67\delta^7 + 133.55\delta^8) \tag{23}$$

It is noted that these above expressions are only valid for values of $\delta = 0.1 - 0.7$ and in the existing model $\delta = 0.6$ is taken. After replacing Eqs. (19) and (20) into Eq. (16), the cracked plate vibration equation is,

$$EI_{eq}\left(\frac{\partial^4 w}{\partial x^4} + 2\frac{\partial^4 w}{\partial x^2 \partial y^2} + \frac{\partial^4 w}{\partial y^4}\right) + I_o\left(V^2 \frac{\partial^2 w}{\partial x^2} + 2V\frac{\partial^2 w}{\partial x \partial t} + \frac{\partial^2 w}{\partial t^2}\right) + \frac{\partial^2 M_T}{\partial x^2} + \frac{\partial^2 M_T}{\partial y^2} \\ - \frac{2a}{3(\frac{a_{bt}}{6} + a_{bb})(3+v)(1-v)h + 2a}\left(EI_{eq}\left(\frac{\partial^4 w}{\partial y^4} + v\frac{\partial^4 w}{\partial x^2 \partial y^2}\right) + \frac{\partial^2 M_T}{\partial y^2}\right) \\ + N_{Tx}\frac{\partial^2 w}{\partial x^2} + N_{Ty}\frac{\partial^2 w}{\partial y^2} + \frac{2a}{(6a_{tb} + a_{tt})(1-v^2)h + 2a}N_{Ty}\frac{\partial^2 w}{\partial y^2} = 0 \tag{24}$$

The effect of thermal bending moment is ignored (i.e. $M_T = 0$) in this work. Then, the final vibration equation for the porosity of the cracked FGM plate under the influence of the thermal environment and moved horizontally is written as follows,

$$EI_{eq}\left(\frac{\partial^4 w}{\partial x^4} + 2\frac{\partial^4 w}{\partial x^2 \partial y^2} + \frac{\partial^4 w}{\partial y^4}\right) + I_o\left(V^2 \frac{\partial^2 w}{\partial x^2} + 2V\frac{\partial^2 w}{\partial x \partial t} + \frac{\partial^2 w}{\partial t^2}\right) \\ - H_1\left(EI_{eq}\left(\frac{\partial^4 w}{\partial y^4} + v\frac{\partial^4 w}{\partial x^2 \partial y^2}\right)\right) + N_{Tx}\frac{\partial^2 w}{\partial x^2} + N_{Ty}\frac{\partial^2 w}{\partial y^2} + H_2 N_{Ty}\frac{\partial^2 w}{\partial y^2} = 0 \tag{25}$$

$$H_1 = \frac{2a}{3(\frac{a_{bt}}{6} + a_{bb})(3+v)(1-v)h + 2a}, \quad H_2 = \frac{2a}{(6a_{tb} + a_{tt})(1-v^2)h + 2a} \tag{26}$$

The boundary conditions of the plate with four edges simply supported are as follows,

$$w(0,y) = 0, \quad w(l_1,y) = 0, \quad \frac{\partial^2 w(0,y)}{\partial x^2} = 0, \quad \frac{\partial^2 w(l_1,y)}{\partial x^2} = 0$$

$$w(x,0) = 0, \quad w(x,l_2) = 0, \quad \frac{\partial^2 w(x,0)}{\partial y^2} = 0, \quad \frac{\partial^2 w(x,l_2)}{\partial y^2} = 0 \tag{27}$$

To simplify the governing equations and before resolving its, the following parameters (dimensionless) are used,

$$W = \frac{w}{h} ; \ X = \frac{x}{l_1} ; \ Y = \frac{y}{l_2} ; \ \lambda = \frac{l_1}{l_2} ;$$

$$T = \frac{th}{l_a^2} \sqrt{\frac{E_c}{12\rho_c(1-v^2)}} ; \ u = \frac{l_1 V}{h} \sqrt{\frac{12\rho_c(1-v^2)}{E_c}} ; \ \lambda_T = \frac{N_T l_a^2}{D_c} \tag{28}$$

Substituting these quantities (dimensionless) into Eq. (25), the vibration equation (dimensionless), yields,

$$\gamma\left(\frac{\partial^4 W}{\partial X^4} + 2\lambda^2 \frac{\partial^4 W}{\partial X^2 \partial Y^2} + \lambda^4 \frac{\partial^4 W}{\partial Y^4} \right) + \alpha\left(u^2 \frac{\partial^2 W}{\partial X^2} + 2u \frac{\partial^2 W}{\partial X \partial T} + \frac{\partial^2 W}{\partial T^2} \right)$$

$$- H_1\gamma\left(\lambda^4 \frac{\partial^4 W}{\partial Y^4} + v\lambda^2 \frac{\partial^4 W}{\partial X^2 \partial Y^2} \right) + \lambda_T \gamma_1 \frac{\partial^2 W}{\partial X^2} + \lambda_T \gamma_1 \lambda^2 \frac{\partial^2 W}{\partial Y^2} + H_2 \lambda_T \gamma_1 \lambda^2 \frac{\partial^2 W}{\partial Y^2} = 0 \tag{29}$$

It is noteworthy that the formula in equation (29), after neglecting thermal parameter, velocity, and physical gradient effect is similar to that suggested by [28], respectively, for isotropic plate. For boundary conditions, the dimensionless form is obtained by substituting Eq. (28) into Eq. (27) gives,

$$W(0,Y) = 0 , \ W(1,Y) = 0 , \ \frac{\partial^2 W(0,Y)}{\partial X^2} = 0 , \ \frac{\partial^2 W(1,Y)}{\partial X^2} = 0 \tag{30}$$

$$W(X,0) = 0 , \ W(X,1) = 0 , \ \frac{\partial^2 W(X,0)}{\partial Y^2} = 0 , \ \frac{\partial^2 W(X,1)}{\partial Y^2} = 0 \tag{31}$$

Assume the solution of equation (29) that satisfies boundary condition Eqs. (30 and 31) be,

$$W(X,Y) = \sum_{m=1}^{\infty} \sum_{n=1}^{\infty} \overline{W}(X) \sin m\pi Y \tag{32}$$

Substituting equation (32) into equation (29), and after rearranging get,

$$\gamma\left(\frac{\partial^4 \overline{W}}{\partial X^4} \right) + \left(\alpha u^2 - 2\lambda^2 m^2 \pi^2 \gamma + H_1 v \lambda^2 m^2 \pi^2 + \lambda_T \gamma_1 \right)\frac{\partial^2 \overline{W}}{\partial X^2} + \alpha 2u \frac{\partial^2 \overline{W}}{\partial X \partial \tau} + \alpha \frac{\partial^2 \overline{W}}{\partial \tau^2}$$

$$+ \left(- H_1\gamma\lambda^4 m^4 \pi^4 + \lambda^4 m^4 \pi^4 \gamma - \lambda_T \gamma_1 \lambda^2 m^2 \pi^2 - H_2 \lambda_T \gamma_1 \lambda^2 m^2 \pi^2 \right)\overline{W} = 0 \tag{33}$$

The boundary condition in Eqs. (31) now be expressed as,

$$\widetilde{W}(0,Y) = 0 , \ \widetilde{W}(1,Y) = 0 , \ \frac{\partial^2 \widetilde{W}(0,Y)}{\partial X^2} = 0 , \ \frac{\partial^2 \widetilde{W}(1,Y)}{\partial X^2} = 0 \tag{34}$$

3. Solution Method

The Differential Quadrature (DQM) Method was utilized as a numerical method for solving the vibration equation (Eq. (33)) as well as the boundary conditions associated (Eq. 34). The essential idea of DQM is to approximate the rth derivative of a function with the value of a weighted sum of the function at all sampling points [29],

$$f_x^{(r)}(\eta) = \sum_{j=1}^{n} A_{ij}^{(r)} f_j , i = 1,2,\dots n \tag{35}$$

Where: $A_{ij}^{(r)}$ is the rth order weight coefficient; f_j is the function value of the function at x_i; n is the number of grid points. Then the derivatives of the modal function with respect to the axial coordinates can be expressed as,

$$\widetilde{W}''''(x_i) = \sum_{j=1}^{n} A_{ij}^{(4)} \widetilde{W}_j \; , \; \widetilde{W}''(x_i) = \sum_{j=1}^{n} A_{ij}^{(2)} \widetilde{W}_j$$

$$\widetilde{W}'(x_i) = \sum_{j=1}^{n} A_{ij}^{(1)} \widetilde{W}_j \; , \; \widetilde{W}'''(x_i) = \sum_{j=1}^{n} A_{ij}^{(3)} \widetilde{W}_j \tag{36}$$

The non-uniform grid points are used to divide the axial direction. At the same time, in order to deal with the boundary conditions, the δ method [29] is introduced, and two grids with a distance of δ (about 10^{-4} ∼ 10^{-6}) from the end points are added at the nodes at both ends,

$$x_1 = 0, x_2 = \delta, x_{n-1} = 1 - \delta, x_n = 1, x_i = \frac{1}{2}\left[1 - \cos\frac{(i-1)\pi}{n-1}\right], i = 3,4,....,n-2 \tag{37}$$

According to the interpolation principle, the Lagrange polynomial is used to determine the weight coefficient [17], and the first-order weight coefficient expression can be obtained,

$$A_{ij}^{(1)} = \begin{cases} \prod_{k=1,k\neq i}^{n}(x_i - x_k)/(x_i - x_j)\prod_{k=1,k\neq j}^{n}(x_j - x_k) \\ i,j = 1,2,....,n, i \neq j \\ \sum_{k=1,k\neq i}^{n}\frac{1}{(x_i - x_k)}; i,j = 1,2,...,n, i = j \end{cases} \tag{38}$$

The governing equation (Eq. 33) for free vibration of FG porous moving plate with crack can be converted into the following expression by substituting the weighting coefficients of required derivatives using DQM above,

$$\gamma\sum_{j=1}^{N}C_{ij}^{(4)}\widetilde{W}_j + \left(\alpha u^2 - 2\lambda^2 m^2 \pi^2 \gamma + H_1 \gamma\nu\lambda^2 m^2 \pi^2 + \lambda_T \gamma_1\right)\sum_{j=1}^{N}C_{ij}^{(2)}\widetilde{W}_j$$

$$+ 2\alpha u\omega_{mn}\sum_{j=1}^{N}C_{ij}^{(1)}\widetilde{W}_j + \begin{pmatrix} -H_1\gamma\lambda^4 m^4 \pi^4 + \lambda^4 m^4 \pi^4 \gamma - \\ \lambda_T\gamma_1\lambda^2 m^2 \pi^2 - H_2\lambda_T\gamma_1\lambda^2 m^2 \pi^2 + \omega_{mn}^2\alpha \end{pmatrix}\widetilde{W} = 0 \tag{39}$$

The DQ-discretized form of the boundary conditions (34) are,

$$\widetilde{W}_n(X_j) = 0, \; (j = 1,.....N_X)$$

$$\sum_{k=1}^{N_x}A_{ik}^{(2)}\widetilde{W}_n(X_k) = 0, \; (j = 2,.......N_X - 1) \tag{40}$$

By utilizing DQM, equation (39) can be converted into assembled form as,

$$\begin{bmatrix} 0 & 0 \\ M_{db} & M_{dd} \end{bmatrix}\begin{Bmatrix} \ddot{w}_b \\ \ddot{w}_d \end{Bmatrix} + \begin{bmatrix} 0 & 0 \\ C_{db} & C_{dd} \end{bmatrix}\begin{Bmatrix} \dot{w}_b \\ \dot{w}_d \end{Bmatrix} + \begin{bmatrix} K_{bb} & K_{bd} \\ K_{db} & K_{dd} \end{bmatrix}\begin{Bmatrix} w_b \\ w_d \end{Bmatrix} = 0 \tag{41}$$

Subscripts b and d represent boundary and internal nodes, respectively. Where K, C, and M are stiffness, damping, and mass matrices respectively.. $\hat{W}$ is a dynamic displacement vector defined by,

$$W = \hat{W}e^{\omega t} \tag{42}$$

The standard generalized eigenvalue problem is obtained by substituting Eq. (42) into Eq. (41) as follows,

$$\{K + \omega C + \omega^2 M\}\hat{W} = 0 \tag{43}$$

The nontrivial solution of Eq. (43) is obtained by equating determinant of coefficient matrix in Eq. (43) to zero,

$$\det\{K + \omega C + \omega^2 M\} = 0 \tag{44}$$

The natural frequencies ω which are complex numbers $\omega = \omega_r + i\omega_i$ can be found using the MATLAB program through solving the characteristic equation referred to in Equation (44). The real parts of the system frequency are related to the vibration frequency while the imaginary parts indicated the damping coefficient of the system.

4. Numerical Analysis and Discussion

In this section, the theoretical results of moving FG porous cracked thin plate obtained by solving the governing equation (44) with associated boundary conditions using the DQM approach are presented and discussed. The dimensions and properties used in numerical results for FG plate are taken as follows [30]: The FGM plate used in this study is composed of aluminum and alumina materials. It is assumed that the FGM plate is made of aluminum metal (k=∞) and alumina ceramics (k=0). Their materials properties are given as: $\rho_c = 3800 \ kg/m^3, \rho_m = 2707 \quad kg/m^3, E_c = 380 \ GPa, \quad E_m = 70 \ GPa$, $\alpha_c = 7.4e - 6K^{-1}$ and $\alpha_m = 23e - 6K^{-1}$, the geometry of the FGM plate is length $(l_1 = 1m)$, width $(l_2 = 1m)$ and thickness $(h = 0.01m)$. This is a thin plate because the width-to-thickness ratio is $l_1 / h = 100$. The Poisson ratio is considered as a constant value $(v = 0.3)$.

4.1. Validation

Some of the theoretical results are compared with published results that have the same parameters for validation of the present method. Table 1 compares the natural frequencies of FGM plate calculated in this paper (DQM) with the results of those reported by [31] for FG plates using (DSM) under (SSSS, and CSCS) boundary conditions with different aspect ratio. The calculation results in this paper are very close to those in the exhibited in Ref. [31]. In this work, The natural ($\overline{\omega}$) frequency (dimensionless) values are defined with respect to the ceramic material as $\overline{\omega} = \omega l_1^2 \sqrt{\rho_c h / D_c}$.

Another validation between the results of the current study using (DQM) was performed with the results obtained by Ref. [32], using the Galerkin method for SSSS isotropic plate as shown in Table 2 with different crack length ratios $(l_c = 2a / l_1 = 0 - 0.2)$. The material properties of the isotropic plates are taken as $E = 207$ GPa, $v = 0.3$, and $\rho = 7850 \ kg/m^3$. The present results of SSSS plates are very close to those obtained [32].

4.2. Parametric analysis

The above two comparative examples verify the reliability and effectiveness of the calculation method in this study. The following analysis analyzes the FGM plate on (SSSS) boundary conditions. The influence of the material composition index k, the axial movement speed u, the aspect ratio, thermal load parameter, porosity parameter, crack length ratio and other factors on the free vibration frequency and stability of the axially moving cracked porosity FGM plate are presented separately.

I. Effect of the Flow Velocity

In this subsection, the impact of moving speed on stability and dimensionless complex frequency of cracked porous moving FG plate was studied. Firstly, Table 3 present the dimensionless vibration frequency as a function of the dimensionless speed movement for moving cracked porosity FG plate, respectively. The results are computed for the case $\beta = 0.2$, $\lambda = 1$; $\lambda_T = 0$ and $l_c = \frac{2a}{l_1} = 0.2$. As shown from this table, with increasing of u the results of the first three vibrations frequency decreased (i.e. the natural frequencies of moving FG plate is dependent on the velocity (u) movement). For example, for SSSS moving FG plate as the speed (dimensionless) rises from 0 to 2, the frequency of the first mode vibration lowers by 26.104% and the percentage decrease for the second mode is 7.018% while for the third mode the percentage decrease for the frequency vibration is 2.98%.

At the same time, we can see from the results that, by increasing the movement speed (without dimensions) from 2 to 3, the vibration frequency first-order decreases by 55.407% for SSSS moving FGM plate and thus the gradient rate increases dramatically. Through the foregoing, we note that increasing the speed of the axial movement to the instability of functionally graded plate so when designing these types of systems it is necessary to choose the appropriate speed to maintain the system stability by taking into account the effect of reducing the speed on the structure stiffness.

Table 1. A comparison of first three dimensionless natural frequency with different aspect ratio for FG plate.

Mode λ		source	S-S-S-S			
			k=0	k=0.5	k=1	k=2
(1,1)	0.5	DQM	12.3370	10.4463	9.4131	8.5581
		DSM [31]	12.3370	10.4463	9.4131	8.5581
	1	DQM	19.7392	16.7141	15.0609	13.6930
		DSM [31]	19.7392	16.7142	15.0610	13.6931
(1,2)	0.5	DQM	19.7392	16.7141	15.0609	13.6930
		DSM [31]	19.7392	16.7142	15.0610	13.6931
	1	DQM	49.3480	41.7853	37.6524	34.2326
		DSM [31]	49.3480	41.7854	37.6524	34.2326
(1,3)	0.5	DQM	32.0762	27.1605	24.4740	22.2512
		DSM [31]	32.0762	27.1605	24.4741	22.2512
	1	DQM	98.6960	83.5707	75.3048	68.4653
		DSM [31]	98.6960	83.5707	75.3048	68.4653

Table 2. Non-dimensional natural frequency ω_{mn} for cracked SSSS isotropic plates.

ω_{mn}	Crack length ratio (2a/l1)	Present Works DQM	Soni et al. [32] (Galerkin method)
(1,1)	0.00	19.7392	19.739
	0.02	19.2741	19.274
	0.10	18.1635	18.163
	0.20	17.5633	17.563
(2,1)	0.00	49.3480	49.348
	0.02	46.7058	46.706
	0.10	40,5592	40,560
	0.20	36.8964	36.897
(1,2)	0.00	49.3480	49.348
	0.02	49.0180	49.018
	0.10	48.3131	48.313
	0.20	47.9361	47.936

II. Effect of gradient index

This subsection demonstrates the effect of the power-law exponent with various parameters on the natural frequencies of moving cracked porous FGM thin plate. First, Figure 6 presented the first three

dimensionless natural frequencies of the FGM plate with the end conditions (simple–simple–simple–simple) at $u = 1, \lambda = 1, \beta = 0.2, l_c = 0.2, \lambda_T = 0$. The results showed that the natural frequencies of the FGM plate are inversely proportional to the gradient index. The decrease in frequencies is due to the fact that an increase in the gradient index means a decrease in the material of the ceramic relative to the metallic substance inside the plate, and the fact that the metal has a lower modulus of elasticity than the modulus of elasticity of the ceramic which makes the plate more flexible (i.e. the stiffness of the plate decreases), which leads to a lower at natural frequencies.

Table 3. First three lower frequencies versus movement speed of porous FG plate.

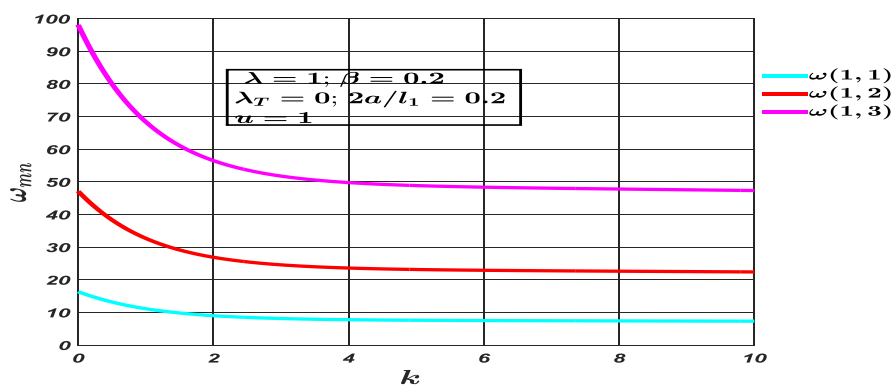| B.C	u	Mode		
		(1,1)	(1,2)	(1,3)
SSSS	0	11.74074	33.2463	68.8937
	1	11.1431	32.7094	68.4095
	2	9.3103	31.0660	66.9467
	3	5.99093	28.2032	64.4708

Figure 6. Impact of power-law exponent on first three real modes of vibration.

The influence of the material composition index k on the first and second order vibration frequency of the SSSS moving FGM porous plate with different crack length ratios ($l_c = 2a/l_1 = 0, 0.1, 0.2, and\ 0.3$) is depicted in Figure 7. In this calculation, let us, $u = 1; \lambda = 1; \beta = 0.2$; and $\lambda_T = 3$. From the plot results in Figure 7, the vibration frequency of the plate gradually decreases with the increase of the material composition index k. This is because the rigidity of metallic materials is relatively small compared to that of non-metallic materials, and the content of metallic materials increases with the material composition index while the contents of ceramics decrease. This, in turn, leads to a gradual decrease in the overall plate rigidity and subsequently a decrease in the frequency of vibration. On the other hand, we note that when the length of the crack is equal to zero, the highest frequencies can be obtained. The natural frequencies of the cracked FGM plate decrease with the increase in the crack length, which means that the increase in the crack length leads to a decrease in the stiffness of the plate structure and thus a decrease in the natural frequencies of vibration for both cases of support.

The effect of volume fraction exponent (k) and moving speed on the first natural frequency of FGM plate for two end conditions with $\lambda_T = 2$; $\lambda = 1$; and $l_c = 2a/l_1 = 0.2$ are shown in Table 4 and Figures (8, a, b and c) . The result indicates that the increase for the moving speed leads to a decrease in natural frequency values for each boundary condition. Also, the vibration frequency of FGM plate will decrease with the increase in the exponent of volume fraction k. The results indicate that the vibration frequency of the FGM plate will increase as the gradient index k increases. For example, for u = 1, porosity index = 0.1 and the SSSS end conditions, the vibration frequency (non-dimensional) decreases from 12.8104 to 8.9672 for (k = 0.5 and k = 2, respectively) (i.e., the percentage drop is 42.858%), while the percentage decrease in vibration frequency for (k = 2 and k = 5) is 8.40%. It is evident from the results that the vibration frequency decreases rapidly at first with increasing gradient index and then gradually slows down. The reason for this is that aluminum content in FGM plate increases, whilst the alumina content decrease with an increasing the exponent, and the alumina Young's modulus is frequently greater than that from aluminum.
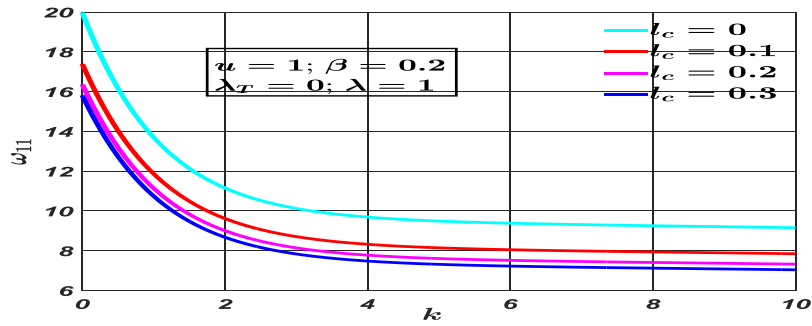
Figure 7. The first and second modes of SSSS FGM plate against exponent k for different values of crack length ratio.

Table 4. Gradient index effect on first frequency of SSSS FG plate with different porosity parameter and moving velocity.

| u	β	k					
		0	0.5	1	2	5	10
0	0	16.4865	13.1061	11.4013	10.092	9.6402	9.3938
	0.1	16.9871	13.3283	11.3445	9.6635	9.0212	8.8759
	0.2	17.5362	13.5320	11.1532	8.8250	7.64593	7.6476
1	0	16.0597	12.5842	10.8087	9.4298	8.9434	8.6764
	0.1	16.5696	12.8104	10.7444	8.9672	8.2719	8.1095
	0.2	17.1294	13.0178	10.5385	8.0603	6.7602	6.7510
2	0	14.7670	14.7670	10.9863	7.3518	6.74747	6.4084
	0.1	15.3072	11.2288	8.8919	6.7746	5.8877	5.6675
	0.2	15.8990	11.4496	8.6400	5.6149	3.8022	3.7739
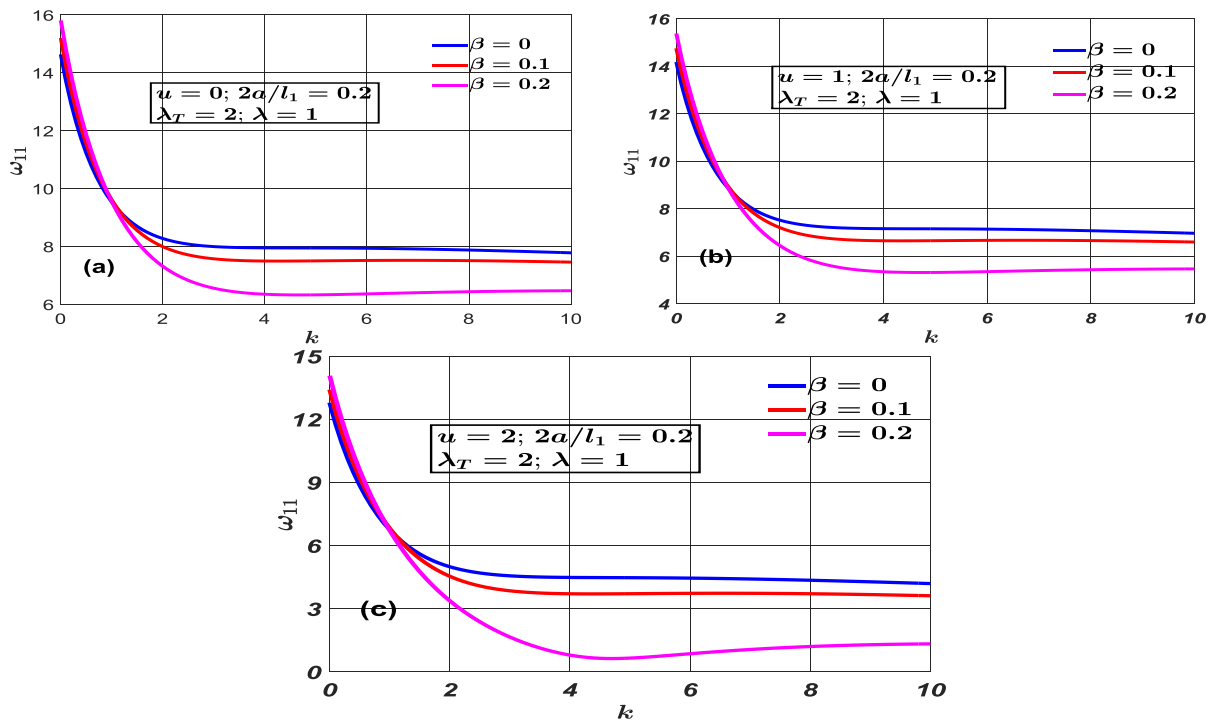
Figure 8. First mode frequency variation of SSSS FG plate with gradient index and porosity for different moving speed.

The effect of the exponent power-law and the porosity parameter of FG plate in different crack length ratio SSSS of the boundary conditions are given in Table 5. The flexure rigidity and elasticity of the graded plates decreases with the increase in the power-law exponent, and because the vibration frequencies are directly proportional to these coefficients. Therefore, an increase in the power-law exponent leads to a decrease in vibration frequencies as shown in the Table 5. Moreover, the first dimensionless frequency variance of SSSS FG plate with gradient index, porosity parameters and for different values of crack length are shown in Figure 9. From these figures it is clear that when the power law exponent is less than 1 approximately, the frequency increases with the increase of the porosity coefficient, while when the gradient index is approximately more than 1, the frequencies decrease with increasing porosity. Also, the results indicate that the increase in the crack length ratio leads to a decrease in natural frequency values for each boundary condition.

Table 5. Gradient index effect on first frequency of SSSS FG plate with different porosity parameter and moving velocity.

$2a/l_1$	β	k					
		0	0.5	1	2	5	10
$l_c=0$	0	18.3127	14.6626	12.7740	11.2858	10.6941	10.3629
	0.1	18.8074	14.8372	12.6271	10.7066	9.8777	9.6429
	0.2	19.3582	14.9921	12.3259	9.6517	8.1645	8.0644
$l_c=0.1$	0	16.9559	13.4205	11.6047	10.1855	9.6556	9.3620
	0.1	17.4573	13.6233	11.5047	9.6744	8.9243	8.7311
	0.2	18.0110	13.8071	11.2584	8.7075	7.3326	7.2834
$l_c=0.2$	0	16.0597	12.5842	10.8087	9.4298	8.9434	8.6764
	0.1	16.5696	12.8104	10.7444	8.9672	8.2719	8.1095
	0.2	17.1294	13.0178	10.5385	8.0603	6.7602	6.7510

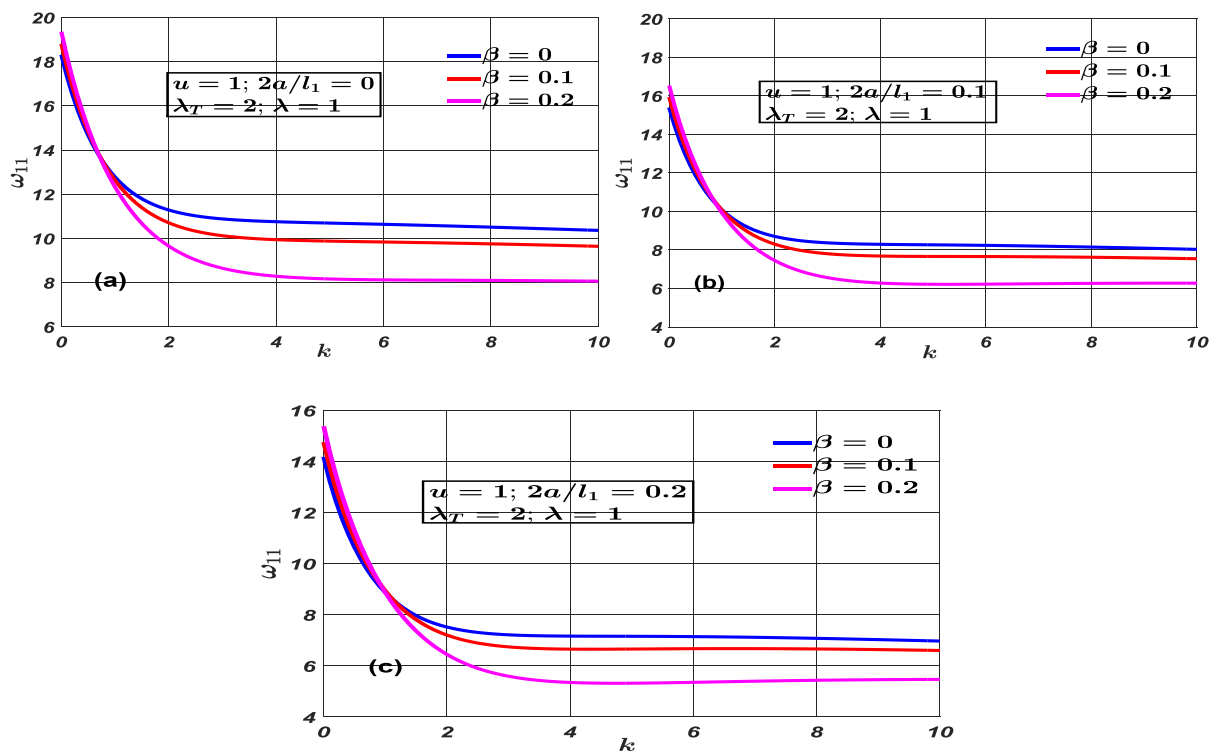Figure 9. First mode frequency of SSSS FG plate with gradient index and porosity for crack length ratio.

III. Crack length ratio effect

The effect of crack length ratio (l_c) and porosity (β) index on the frequencies (non-dimensional) of FG plate with two boundary conditions and thickness $l_1/h = 100$ is demonstrated in Table 6 and Figure 10. In the calculation, let ($k = 1$, $\lambda = 1$, $u = 1$, and $\Delta T = 0$). From the results presented in this table and figure, it is seen that for constant porosity that frequency decrease with increasing crack length (l_c) ratio. Also, it is noted that as the porosity parameter (β) increases, the vibration first frequency decreases with a constant length crack ratio. This is because the increase in the percentage of porosity and the length of the crack increases the local flexibility, and then there is a decrease in the stiffness of the plate.

Table 6. Impact of crack length ratio of vibration frequency with different porosity parameter.

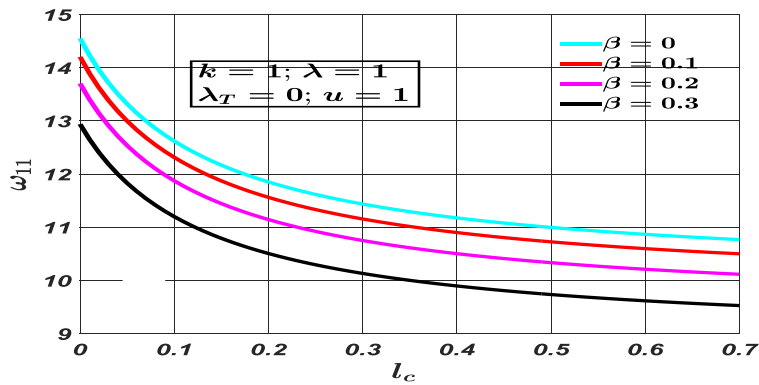| B.C.	β	l_c				
		0	0.1	0.2	0.3	0.5
	0	14.5505	13.5963	12.9791	12.5460	11.9768
SSSS	0.1	14.2032	13.2695	12.6655	12.2416	11.6844
	0.2	13.7029	12.7986	12.213	11.8029	11.2631
	0.3	12.9388	12.0792	11.5229	11.1323	10.6188

Figure 10. First mode frequency variation for moving FG plate versus crack length ratio under different porosity factor; for SSSS.

Table 7 and Figure 11 show the crack length ratio l_c and gradient index k effects on the first-order natural frequency of SSSS FGM plate. From the results is exhibited that the increase in crack length leads to a decrease in frequency. The stiffness of the plate decreases in the presence of the crack, and thus the frequencies decrease because the length of the crack is in the opposite sense of the frequency, and the crack increases the local flexibility. Moreover, it is noticed that the frequency decreases with increasing (k) gradient index. This can be expounded by the increase in the volume fraction of the metallic as a result of the stiffness reduction. It can also be seen that the decrease in the frequency is due to the combined effect of increasing the crack length, and gradient index.

Table 7. Effect of the crack length ratio, the gradient index on the first (dimensionless) frequency for FG plate ($\lambda_T = 0$; $u = 1$; $\lambda = 1$; and $\beta = 0.2$).

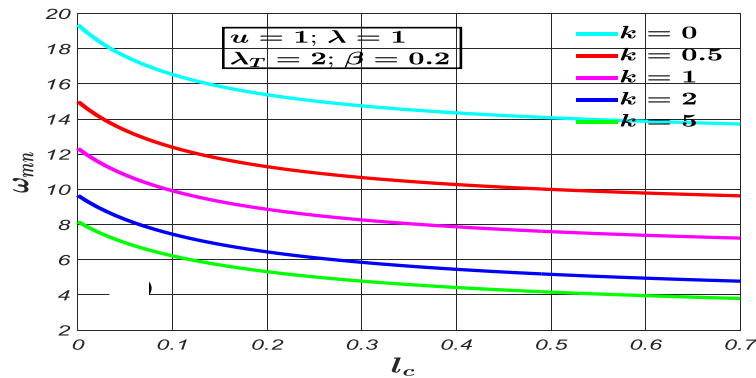| BC	k	l_c				
		0	0.1	0.2	0.3	0.5
	0	19.9810	18.7016	17.8749	17.2952	16.5340
	0.5	16.1704	15.1201	14.4410	13.96459	13.3386
SSSS	1	13.7029	12.7986	12.2136	11.8029	11.2631
	2	11.1548	10.3981	9.9081	9.5637	9.1107
	5	9.4915	8.8285	8.3985	8.0961	7.6977

Figure 11. Crack length ratio, the gradient index impact on the first (dimensionless) frequency for (SSSS) FG plate movement.

5. Conclusion

The free vibration of the axially moving porous FGM thin plate with cracks is analyzed in this article. Based on the classical plate theory, the motion equation of the axially moving FGM plate is derived, and differential quadrature methods are used to solve the vibration equation. The reliability and effectiveness of the calculation method in this article are verified by comparison examples. The influence of axial motion speed, crack length ratio, material composition index on the vibration frequency are discussed through parameter analysis. The result analysis shows,

1. For porous FG plates with axial motion and crack, increasing the porosity index first yields an increase in vibration frequency for a small value of k, then this trend becomes opposite for upper values of gradient index k.
2. Compared with the intact moving FG plate, the crack length of the cracked moving FG plate reduces the critical buckling speed and coupled-mode flutter of the FGM plate. The greater the crack length, the lower the critical buckling speed and coupled-mode flutter of the FGM plate. The faster the plate will undergo flutter instability, mainly because the crack reduces the overall stiffness of the FGM plate.
3. As the length of the crack increases, the stiffness of the plate decreases due to the energy released by the crack sites, and thus the vibration plate's frequency decreases.
4. The stability of axially moving plates is highly dependent on the variation in axial speed. With an increase in the speed of movement, the frequency of vibration decreases faster. Hence, system instability occurs as a result of increased speed.

References

[1]   D. G. Zhang and Y. H. Zhou, "A theoretical analysis of FGM thin plates based on physical neutral surface," Comput. Mater. Sci., vol. 44, no. 2, pp. 716–720, 2008, doi: 10.1016/j.commatsci.2008.05.016.
[2]   X. Zhao, Y. Y. Lee, and K. M. Liew, "Free vibration analysis of functionally graded plates using the element-free kp-Ritz method," J. Sound Vib., vol. 319, no. 3–5, pp. 918–939, 2009, doi: 10.1016/j.jsv.2008.06.025.
[3]   S. Chakraverty and K. K. Pradhan, "Free vibration of exponential functionally graded rectangular plates in thermal environment with general boundary conditions," Aerosp. Sci. Technol., vol. 36, pp. 132–156, 2014, doi: 10.1016/j.ast.2014.04.005.
[4]   M. C. Kiran and S. C. Kattimani, "Assessment of porosity influence on vibration and static behaviour of functionally graded magneto-electro-elastic plate: A finite element study," Eur. J. Mech. A/Solids, vol. 71, no. April, pp. 258–277, 2018, doi: 10.1016/j.euromechsol.2018.04.006.
[5]   A. S. Rezaei and A. R. Saidi, "Exact solution for free vibration of thick rectangular plates made of porous materials," Compos. Struct., 134, pp. 1051–1060, 2015, doi: 10.1016/j.compstruct.2015.08.125.
[6]   A. S. Rezaei, A. R. Saidi, M. Abrishamdari, and M. H. P. Mohammadi, "Natural frequencies of functionally graded plates with porosities via a simple four variable plate theory: An analytical approach," Thin-Walled Struct., vol. 120, no. May, pp. 366–377, 2017, doi: 10.1016/j.tws.2017.08.003.
[7]   Y. F. Zhou and Z. M. Wang, "Transverse vibration characteristics of axially moving viscoelastic plate," Appl. Math. Mech. (English Ed., vol. 28, no. 2, pp. 209–218, 2007, doi: 10.1007/s10483-007-0209-1.
[8]   Y. Q. Wang and J. W. Zu, "Nonlinear dynamics of a translational FGM plate with strong mode interaction," Int. J. Struct. Stab. Dyn., vol. 18, no. 03, p. 1850031, 2018, doi: 10.1142/S0219455418500311.
[9]   G. Yao and Y.-M. Zhang, "Dynamics and stability of an axially moving plate interacting with surrounding airflow," Meccanica, vol. 51, no. 9, pp. 2111–2119, 2016.

[10] Y. Q. Wang and J. W. Zu, "Nonlinear dynamic thermoelastic response of rectangular FGM plates with longitudinal velocity," Compos. Part B Eng., vol. 117, pp. 74–88, 2017, doi: 10.1016/j.compositesb.2017.02.037.

[11] Y. Q. Wang, S. W. Xue, X. B. Huang, and W. Du, "Vibrations of axially moving vertical rectangular plates in contact with fluid," Int. J. Struct. Stab. Dyn., vol. 16, no. 02, p. 1450092, 2016, doi: 10.1142/S0219455414500928.

[12] G. Yao, Y.-M. M. Zhang, C.-Y. Y. Li, and Z. Yang, "Stability analysis and vibration characteristics of an axially moving plate in aero-thermal environment," Acta Mech., vol. 227, no. 12, pp. 3517–3527, 2016, doi: 10.1007/s00707-016-1674-6.

[13] X. X. Guo, "Thermoelastic coupling vibration of the moving rectangular plate," Appl. Mech. Mater., vol. 319, pp. 435–439, 2013, doi: 10.4028/www.scientific.net/AMM.319.435.

[14] E. K. Njim, S. H. Bakhy, and M. Al-Waily, "Analytical and Numerical Investigation of Free Vibration Behavior for Sandwich Plate with Functionally Graded Porous Metal Core," Pertanika J Sci. Technol., vol. 29, no. 3, pp. 1655–1682, 2021, doi: 10.47836/pjst.29.3.39.

[15] E. K. Njim, S. H. Bakhy, and M. Al-Waily, "Analytical and numerical free vibration analysis of porous functionally graded materials (Fgpms) sandwich plate using rayleigh-ritz method," Arch. Mater. Sci. Eng., vol. 110, no. 1, pp. 27–41, 2021, doi: 10.5604/01.3001.0015.3593.

[16] RICE and LEVY N, "Part-Through Surface Crack in an Elastic Plate," ASME Pap, no. xi, pp. 185–194, 1971.

[17] T. Bose and A. R. Mohanty, "Vibration analysis of a rectangular thin isotropic plate with a part-through surface crack of arbitrary orientation and position," J. Sound Vib., vol. 332, no. 26, pp. 7123–7141, 2013, doi: 10.1016/j.jsv.2013.08.017.

[18] S. E. Khadem and M. Rezaee, "Analytical approach for obtaining the location and depth of an all-over part-through crack on externally in-plane loaded rectangular plate using vibration analysis," J. Sound Vib., vol. 230, no. 2, pp. 291–308, 2000, doi: 10.1006/jsvi.1999.2619.

[19] M. J. Jweeg, A. S. Hammood, and M. Al-Waily, "A suggested analytical solution of isotropic composite plate with crack effect," Int. J. Mech. Mechatronics Eng., vol. 12, no. 5, pp. 44–58, 2012.

[20] N. A. Bachaya and T. Eh. Elaikh, "Transverse Vibration of Cracked Graded Rayleigh Beam with Axial Motion," Univ. Thi-Qar J. Eng. Sci., vol. 11, 2021, doi: 10.31663/tqujes.11.2.390(2021).

[21] G. D. R. P.V.Joshi , N.K.Jain, "Effect of thermal environment on free vibration of cracked rectangular plate: Ananalytical approach," Thin-Walled Struct., no. 91, pp. 38–49, 2015.

[22] Y. S. Al Rjoub and J. A. Alshatnawi, "Free vibration of functionally-graded porous cracked plates," Structures, vol. 28, no. October, pp. 2392–2403, 2020, doi: 10.1016/j.istruc.2020.10.059.

[23] B. Fahsi, R. B. Bouiadjra, A. Mahmoudi, S. Benyoucef, and A. Tounsi, "Assessing the Effects of Porosity on the Bending, Buckling, and Vibrations of Functionally Graded Beams Resting on an Elastic Foundation by Using a New Refined Quasi-3D Theory," Mech. Compos. Mater. vol. 55, no. 2, pp. 219–230, 2019, doi: 10.1007/s11029-019-09805-0.

[24] M. I. Ali and M. S. Azam, "Exact solution by dynamic stiffness method for the natural vibration of porous functionally graded plate considering neutral surface," Proc. Inst. Mech. Eng. Part L J. Mater. Des. Appl., vol. 235, no. 7, pp. 1585–1603, 2021, doi: 10.1177/1464420720988170.

[25] P. V. Joshi, N. K. Jain, G. D. Ramtekkar, and G. Singh Virdi, "Vibration and buckling analysis of partially cracked thin orthotropic rectangular plates in thermal environment," Thin-Walled Struct., vol. 109, no. September, pp. 143–158, 2016, doi: 10.1016/j.tws.2016.09.020.

[26] S. Soni, N. K. Jain, and P. V. Joshi, "Stability and dynamic analysis of partially cracked thin orthotropic microplates under thermal environment: an analytical approach," Mech. Based Des. Struct. Mach., vol. 48, no. 3, pp. 299–325, 2020, doi: 10.1080/15397734.2019.1620613.

[27] P. V. Joshi, N. K. Jain, and G. D. Ramtekkar, "Analytical modeling for vibration analysis of thin rectangular orthotropic/functionally graded plates with an internal crack," J. Sound Vib., vol. 344, pp. 377–398, 2015, doi: 10.1016/j.jsv.2015.01.026.

[28] P. V. Joshi, N. K. Jain, and G. D. Ramtekkar, "Analytical modeling and vibration analysis of internally cracked rectangular plates," J. Sound Vib., vol. 333, no. 22, pp. 5851–5864, 2014, doi: 10.1016/j.jsv.2014.06.028.

[29] E. R. B, T. Eh El, and S.M.H, "Differential Quadrature Method for Dynamic behavior of Function Graded Materials pipe conveying fluid on visco-elastic foundation," Univ. Thi-Qar J. Eng. Sci., vol. 10, no. 1, 2019, doi: 10.31663/tqujes.10.1.352(2019).

[30] S. Merdaci, H. M. Adda, B. Hakima, R. Dimitri, and F. Tornabene, "Higher-Order Free Vibration Analysis of Porous Functionally Graded Plates," J. Compos. Sci., vol. 5, no. 11, p. 305, 2021, doi: 10.3390/jcs5110305.

[31] Y. Wang, Z. Tian, J. Wu, X. Guo, and M. Shao, "Dynamic stability of an axially moving paper board with added subsystems," J. Low Freq. Noise, Vib. Act. Control, vol. 37, no. 1, pp. 48–59, 2018.

[32] S. Soni, N. K. Jain, and P. V. Joshi, "Vibration analysis of partially cracked plate submerged in fluid," J. Sound Vib., vol. 412, pp. 28–57, 2018, doi: 10.1016/j.jsv.2017.09.016.